Hubbard Dimer Green's Function: Exact, G0W0 and scGW

1 Exact Solution : Basis and Operators

We will explain the Python implementation of the exact Green's-function and spectral-function calculation for a two-site Hubbard dimer at quarter filling (one up electron). The code works in the full Fock basis of four spin-orbitals (site $1\uparrow$, site $1\downarrow$, site $2\uparrow$, site $2\downarrow$), i.e. a 16-dimensional many-body space.

1.1 Fock-space dimension

We set:

```
basis_size = 16  # 2^4 configurations for 4 orbitals
```

Four spin-orbitals $\Rightarrow 2^4 = 16$ occupation-number states.

1.2 Creation operator: `create_op(p)`

This function builds the 16×16 matrix for the fermionic creation operator $c_p^\dagger$ in the Fock basis:

```
def create_op(p):
    """Return the creation operator matrix for orbital p in the 16-dim
       Fock basis."""
    mat = np.zeros((basis_size, basis_size), dtype=complex)
    for s in range(basis_size):                          # loop over basis
       states (0  15  )
        if not (s & (1 << p)):                           # if orbital p is
           empty in state s
            # fermion sign from parity of lower bits
            sign = (-1)**bin(s & ((1 << p) - 1)).count("1")
            s_new = s | (1 << p)                        # set bit p     new
               state index
            mat[s_new, s] = sign                        # matrix element
                 s_new  | c _p | s
    return mat
```

- `s` is an integer whose binary bits encode occupations of the 4 orbitals.
- `(1 << p)` is a mask with a 1 in bit position p.
- `s & (1<<p)` tests if bit p is already occupied.
- `bin(...)  .count("1")` counts how many lower bits are set to get the fermionic sign.
- `s_new = s | (1<<p)` flips bit p from 0 to 1.

- The resulting matrix `mat` satisfies

$$(c_p^\dagger)_{s_{\text{new}},s} = (-1)^{\#\{\text{occupied}<p\}}, \quad (c_p^\dagger)_{\cdot,s} = 0 \text{ otherwise.}$$

1.3 Annihilation operators

Once `c_dag` holds creation matrices, annihilation operators are their Hermitian adjoints:

```
c_dag = [create_op(p) for p in range(4)]
c = [op.conj().T for op in c_dag]    # c[p] = (c_dag[p])^
```

Each `c_dag[p]` and `c[p]` is 16×16.

1.4 Number operators

Define on-site number operators

$$n_p = c_p^\dagger c_p$$

in code:

```
n_op = [c_dag[p] @ c[p] for p in range(4)]
# n_op[p] is the 16 16  number matrix for orbital p
```

2 Hamiltonian Construction

The full many-body Hamiltonian is built in Fock space:

```
# zero matrix
H = np.zeros((basis_size, basis_size), dtype=complex)

# hopping term: -t sum_{  }(  c _ {1  } c_{2  } + h.c. )
H += -t * (c_dag[0] @ c[2] + c_dag[2] @ c[0]
            + c_dag[1] @ c[3] + c_dag[3] @ c[1])

# interaction: U (n_{1   }n_{1   } + n_{2   }n_{2   })
H += U * (n_op[0] @ n_op[1] + n_op[2] @ n_op[3])

# orbital energies:      _p   n_p
H += epsilon * sum(n_op)
```

3 Diagonalization and States Extraction

3.1 Solve eigenproblem

```
E, V = np.linalg.eigh(H)    # eigenvalues E (length 16) and eigenvectors V
    (16 16 )
```

3.2 Total number operator

```
N_tot = sum(n_op)
```

3.3 Identify sectors by particle number

Use expectation of N_{tot} to pick out vacuum, 1-electron, 2-electron states:

```
def find_states_by_N(N):
    idxs = []
    for idx in range(basis_size):
        v = V[:, idx]
        n_val = np.real(v.conj().T @ (N_tot @ v))
        if abs(n_val - N) < 1e-6:
            idxs.append(idx)
    return idxs

idx_0 = find_states_by_N(0)[0]
idx_1 = sorted(find_states_by_N(1), key=lambda i: E[i])[0]
idx_2 = find_states_by_N(2)

psi0 = V[:, idx_0]; E0 = E[idx_0]
psi1 = V[:, idx_1]; E1 = E[idx_1]
psi2_list = [V[:, i] for i in idx_2]
E2_list   = [E[i] for i in idx_2]
```

4 Green's Function via Lehmann Representation

Define frequency grid and small broadening η:

```
omega = np.linspace(-10,10,2000)
eta   = 0.05
```

Compute the one-particle Green's function at site/orbital p:

```
def compute_G(p_index):
    G = np.zeros_like(omega, dtype=complex)
    # hole part (removal)
    amp_rem = np.vdot(psi0, c[p_index] @ psi1)
    G += (abs(amp_rem)**2) / (omega - (E1-E0) - 1j*eta)
    # particle part (addition)
    for psi2, E2 in zip(psi2_list, E2_list):
        amp_add = np.vdot(psi2, c_dag[p_index] @ psi1)
        G += (abs(amp_add)**2) / (omega - (E2-E1) + 1j*eta)
    return G

G_up   = compute_G(p_index=0)
G_down = compute_G(p_index=1)
```

Spectral functions:

```
A_up   = -1/np.pi * np.imag(G_up)
A_down = -1/np.pi * np.imag(G_down)
```

5 Limiting cases

5.1 N=2 exact energies from our previous derivation

Recall from previous lectures:

Table 1: Two-electron sector eigenvalues and eigenstates

Eigenvalue	Eigenstate	Description
$2\epsilon + \frac{U}{2} - \sqrt{\left(\frac{U}{2}\right)^2 + 4t^2}$	$\frac{\lvert\uparrow\downarrow,0\rangle + \lvert 0,\uparrow\downarrow\rangle + X\frac{\lvert\uparrow,\downarrow\rangle - \lvert\downarrow,\uparrow\rangle}{\sqrt{2}}}{\sqrt{2+X^2}}$	Ground state (Singlet)
$2\epsilon + U$	$\frac{\lvert\uparrow\downarrow,0\rangle - \lvert 0,\uparrow\downarrow\rangle}{\sqrt{2}}$	Singlet excited state
$2\epsilon + \frac{U}{2} + \sqrt{\left(\frac{U}{2}\right)^2 + 4t^2}$	$\frac{\lvert\uparrow\downarrow,0\rangle + \lvert 0,\uparrow\downarrow\rangle - \frac{1}{X}\frac{\lvert\uparrow,\downarrow\rangle - \lvert\downarrow,\uparrow\rangle}{\sqrt{2}}}{\sqrt{2+1/X^2}}$	Singlet excited state
2ϵ	$\lvert\uparrow,\uparrow\rangle$	Triplet state ($S=1, S_z=+1$)
2ϵ	$\lvert\downarrow,\downarrow\rangle$	Triplet state ($S=1, S_z=-1$)
2ϵ	$\frac{\lvert\uparrow,\downarrow\rangle + \lvert\downarrow,\uparrow\rangle}{\sqrt{2}}$	Triplet state ($S=1, S_z=0$)

5.2 Non-interacting limit ($U = 0$)

One-electron sector. The single-particle Hamiltonian

$$H_{1e} = \begin{pmatrix} \epsilon & -t \\ -t & \epsilon \end{pmatrix}$$

diagonalizes to

$$E_1 = \epsilon - t, \quad E_2 = \epsilon + t,$$

with eigenvectors

$$|\psi_1\rangle = \frac{1}{\sqrt{2}}\begin{pmatrix} 1 \\ 1 \end{pmatrix}, \quad |\psi_2\rangle = \frac{1}{\sqrt{2}}\begin{pmatrix} -1 \\ 1 \end{pmatrix}.$$

Two-electron sector. For $U = 0$, two electrons fill these orbitals independently, giving possible energies

$$2(\epsilon - t), \quad (\epsilon - t) + (\epsilon + t) = 2\epsilon, \quad 2(\epsilon + t).$$

Green's function. The exact one-particle Green's function reduces to the non-interacting form

$$G_{ij}^{\sigma}(\omega) = \sum_{\alpha=\pm} \frac{\psi_{i\alpha}\,\psi_{j\alpha}^{*}}{\omega - (\epsilon + \alpha t) + i\eta}, \quad \psi_{i\alpha} = \frac{1}{\sqrt{2}}.$$

Spectral function. The on-site spectral function is

$$A_{ii}(\omega) = -\frac{1}{\pi}\,\mathrm{Im}\,G_{ii}(\omega) = \frac{1}{2}\Big[\delta\big(\omega - (\epsilon - t)\big) + \delta\big(\omega - (\epsilon + t)\big)\Big].$$

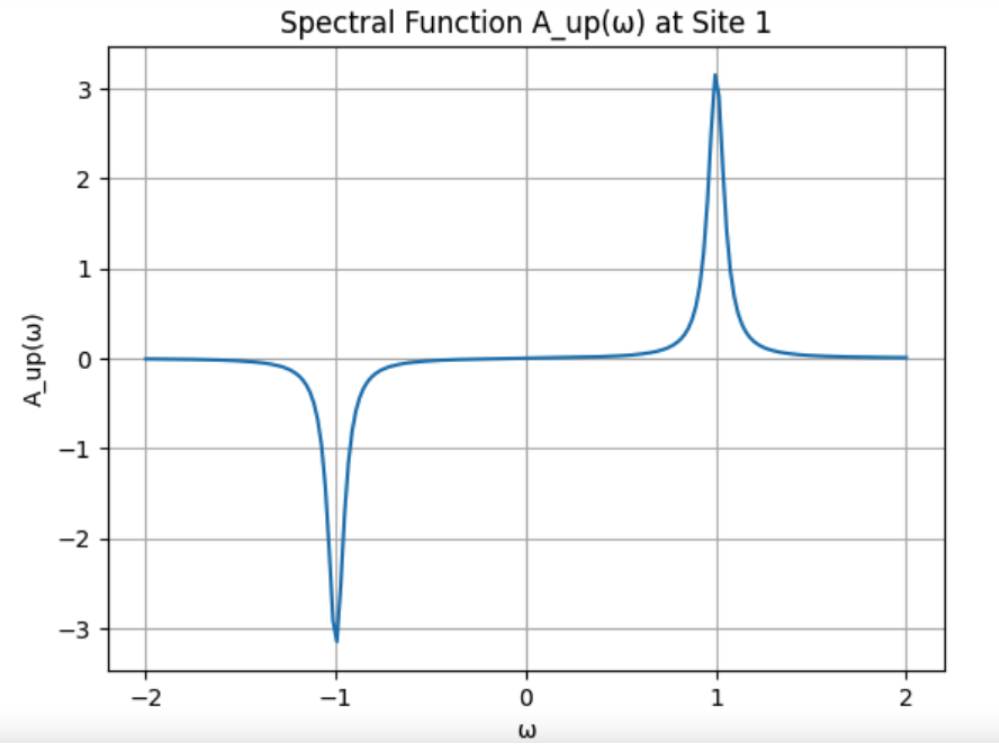

Figure 1: Two site Hubbard model at Quarter filling, U=0, spin up spectral function.

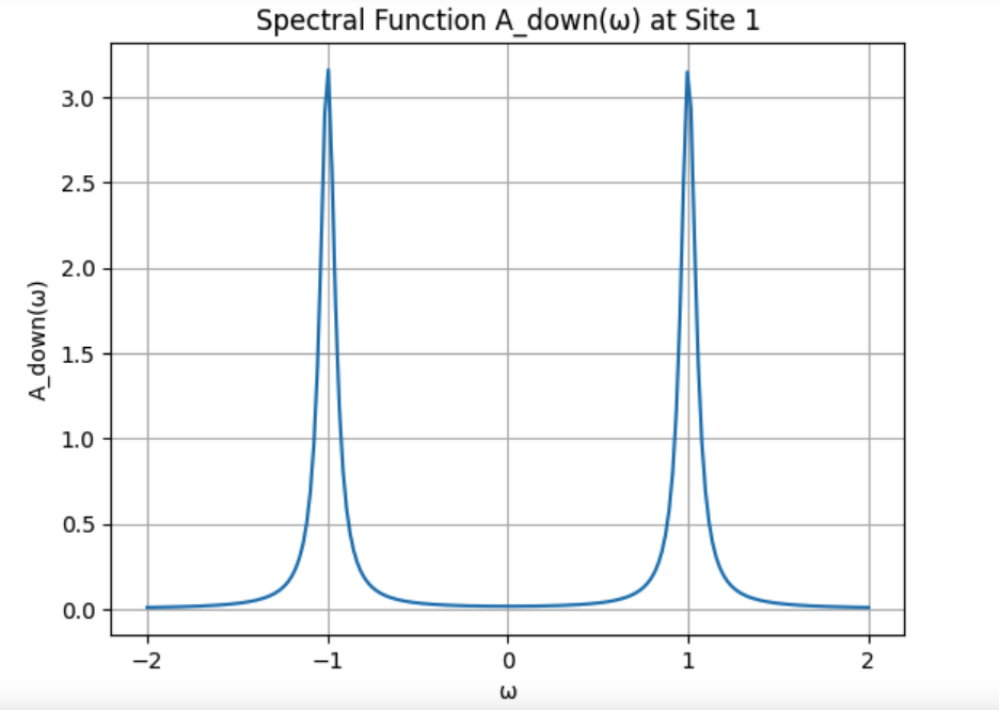

Figure 2: Two site Hubbard model at Quarter filling, U=0, spin down spectral function.

5.3 Strongly interacting limit ($U \gg t$)

In the limit $U \gg t$ the two-site Hubbard dimer approaches the *atomic* regime, with electrons essentially localized on individual sites. One can obtain the leading corrections by expanding the exact eigenvalues in powers of t/U.

Two-electron singlet levels. From the exact expressions (Table 2),

$$E_{\pm} = 2\epsilon + \frac{U}{2} \pm \frac{1}{2}\sqrt{U^2 + 16\,t^2},$$

expand for $U \gg t$:

$$\sqrt{U^2 + 16\,t^2} = U\sqrt{1 + \frac{16\,t^2}{U^2}} \approx U + \frac{8\,t^2}{U},$$

so

$$E_- \approx 2\epsilon + \frac{U}{2} - \frac{1}{2}\Big(U + \tfrac{8\,t^2}{U}\Big) = 2\epsilon - \frac{4\,t^2}{U}, \quad E_+ \approx 2\epsilon + U + \frac{4\,t^2}{U}.$$

Triplet levels. The three triplet states remain degenerate at

$$E_{\text{triplet}} = 2\epsilon,$$

up to corrections of order $\mathcal{O}(t^4/U^3)$.

Superexchange splitting. The singlet–triplet splitting in the low-energy manifolds is

$$J \;\equiv\; E_{\text{triplet}} - E_- \;\approx\; \frac{4\,t^2}{U},$$

This $J \propto t^2/U$ is the familiar superexchange energy in second-order perturbation theory.

Spectral function. In the two-electron sector one finds three addition energies

$$\omega_- \;\approx\; (2\epsilon - E_{1e}) - \frac{4t^2}{U}, \quad \omega_0 \;\approx\; 2\epsilon - E_{1e}, \quad \omega_+ \;\approx\; (2\epsilon - E_{1e}) + U + \frac{4t^2}{U},$$

corresponding respectively to the lower-singlet, middle-triplet, and upper-singlet states. However, since the ground state for $N = 1$ carries a single spin-up electron,

$$\langle \psi^{(2)}_{\text{triplet}} |\, c^\dagger_{1\downarrow}\, |\psi^{(1)}_0\rangle = 0,$$

only the two singlet transitions have nonzero overlap. Thus the spin-down addition spectral function exhibits poles at ω_- and ω_+ (the two singlet peaks), whereas the intermediate triplet pole at ω_0 carries zero spectral weight and does not appear in the spectrum.

In the strict atomic limit $t \to 0$ these collapse to two "Hubbard bands" at $\omega = 2\epsilon - E_{1e}$ and $\omega = 2\epsilon - E_{1e} + U$, each split by the small superexchange scale $\sim 4t^2/U$.

Physical intuition for the superexchange scale $J \sim 4t^2/U$. In the limit $U \gg t$, real hopping of electrons between sites is energetically costly (it would create a doubly-occupied site at energy U). However, *virtual* hopping processes of second order in t still occur:

- Start in a state with one electron on each site ($|\uparrow, \downarrow\rangle$ or its spin-flipped partner).
- One electron *virtually* hops to the other site (amplitude t), creating a doubly-occupied site and paying energy U.
- It then hops back (another factor t), returning to one electron per site.

Because of the Pauli principle, only the *singlet* combination $\frac{1}{\sqrt{2}}(|\uparrow, \downarrow\rangle - |\downarrow, \uparrow\rangle)$ can undergo this virtual double-occupation. The triplet states cannot occupy the same site with opposite spin, so they do not gain this second-order energy lowering.

By second-order perturbation theory, the energy shift for the singlet relative to the triplet is

$$J \;=\; \frac{t^2}{U/4} \;=\; \frac{4\,t^2}{U}\,.$$

Equivalently, one can show the low-energy effective Hamiltonian is the antiferromagnetic Heisenberg coupling

$$H_{\text{eff}} = J\,\mathbf{S}_1 \cdot \mathbf{S}_2, \qquad J = \frac{4\,t^2}{U}.$$

Thus the "superexchange" scale J emerges as the energy splitting between singlet and triplet configurations, reflecting virtual hops suppressed by the large on-site repulsion.

Standard G_0W_0 (or any GW without vertex corrections) will *not* generate the $J \sim 4t^2/U$ singlet–triplet splitting in the large-U regime. Physically, superexchange is a *two-particle* correlation effect: it comes from virtual hops that involve the simultaneous motion of two electrons (and their spin-exchange), which shows up in a four-point vertex. GW only resums bubble diagrams in W and neglects the vertex Γ that couples those bubbles to the fermions, so it cannot distinguish singlet vs. triplet virtual processes and thus leaves the two low-energy levels degenerate.

To capture J you need to go beyond GW—e.g. include at least a ladder or Bethe–Salpeter vertex in the self-energy (GWΓ, T-matrix, or an effective Heisenberg mapping)—so that the virtual-hopping exchange channel is treated correctly.

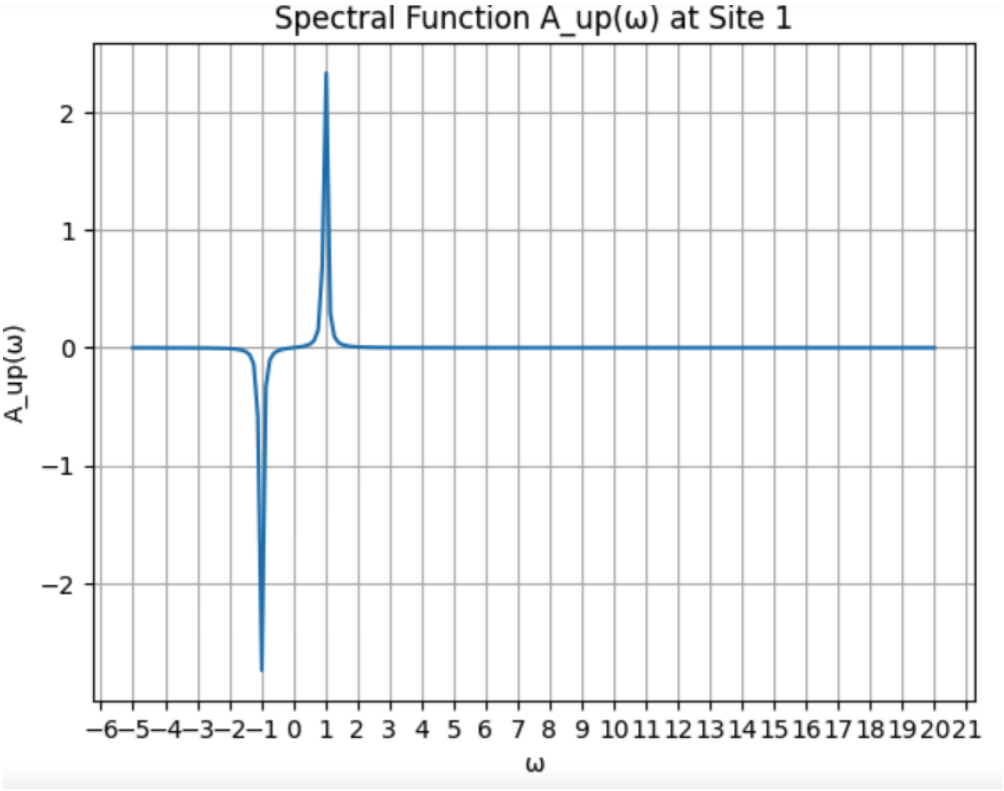

Figure 3: Two site Hubbard model at Quarter filling, U=10, t=1, spin up spectral function.

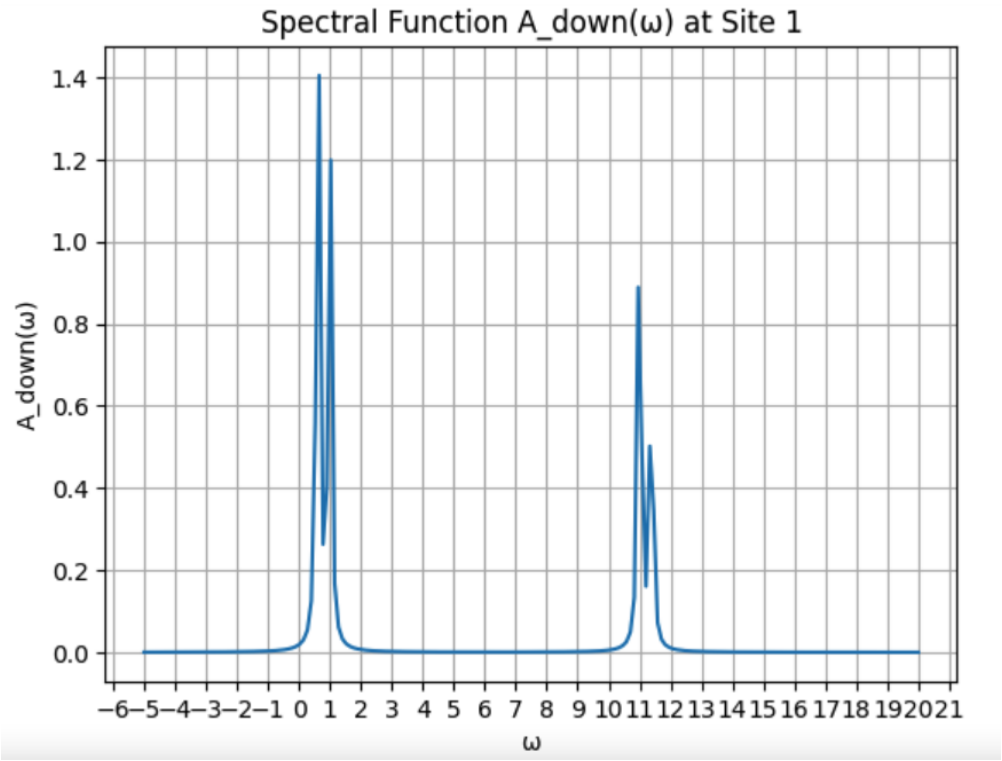

Figure 4: Two site Hubbard model at Quarter filling, U=10, t=1 spin down spectral function.

6 Implementation of the G_0W_0 Approximation

In this section we detail the Python code used to compute the G_0W_0 Green's function and spectral function for the two-site Hubbard dimer. We assume the tight-binding parameters ϵ, t, Hubbard U, and a small broadening η are defined at the top of the script.

6.1 Non-interacting Green's function $G_0(\omega)$

We work in the site basis $\{1, 2\}$. The molecular-orbital energies are $\epsilon \pm t$, and

$$G_0(\omega) = \sum_{\alpha=\pm} \frac{|\psi_\alpha\rangle\langle\psi_\alpha|}{\omega - (\epsilon + \alpha\, t) + i\eta}$$

becomes in matrix form:

$$G_0(\omega) = \begin{pmatrix} G_{00} & G_{01} \\ G_{01} & G_{00} \end{pmatrix}, \quad G_{00} = \tfrac{1}{2}\big(G_+ + G_-\big), \quad G_{01} = \tfrac{1}{2}\big(-G_+ + G_-\big),$$

where $G_\pm = 1/[\omega - (\epsilon \pm t) + i\eta]$. In code:

Listing 1: Non-interacting Green's function

```
def G0_matrix(omega):
    ep1, ep2 = epsilon - t, epsilon + t
    Gp = 1.0/(omega - ep1 + 1j*eta)
    Gm = 1.0/(omega - ep2 + 1j*eta)
    G00 = 0.5*(Gp + Gm)
    G01 = 0.5*(-Gp + Gm)
    return np.array([[G00, G01],
                     [G01, G00]], dtype=complex)
```

6.2 Analytic self-energies $\Sigma_\sigma(\omega)$

Using the RPA-screened interaction in the one-shot G_0W_0 scheme, the self-energy for spin-up has no Hartree term, while spin-down carries a static shift $U/2$. Defining

$$h = \sqrt{(4t)^2 + U^2}\,,$$

we implement:

Listing 2: GW self-energies from analytic formulas

```
def Sigma_up_matrix(omega):
    pref = (U**2 * t) / (4*h)
    pole1 = omega - (epsilon + t + h) + 1j*eta
    pole2 = omega - (epsilon - t - h) - 1j*eta
    s11 = pref*(1/pole1 + 1/pole2)
    s12 = pref*(1/pole1 - 1/pole2)
    return np.array([[s11, s12],
                     [s12, s11]], dtype=complex)

def Sigma_down_matrix(omega):
    vH = U/2
    pref = (U**2 * t) / (4*h)
```

```
    pole1 = omega - (epsilon + t + h) + 1j*eta
    pole2 = omega - (epsilon - t + h) + 1j*eta
    s11 = vH + pref*(1/pole1 + 1/pole2)
    s12 = pref*(1/pole1 - 1/pole2)
    return np.array([[s11, s12],
                     [s12, s11]], dtype=complex)
```

6.3 Dyson equation and spectral function

For each frequency value ω, we solve the Dyson equation

$$G_\sigma(\omega) = \left[G_0^{-1}(\omega) \; - \; \Sigma_\sigma(\omega)\right]^{-1},$$

then extract the on-site spectral function

$$A_\sigma(\omega) = -\frac{1}{\pi} \operatorname{Im} G_{\sigma,11}(\omega).$$

Listing 3: Dyson solve and spectral function

```
# Precompute inverse of G0 and allocate arrays
omega = np.linspace(-10,10,2000)
A_up   = np.zeros_like(omega)
A_down = np.zeros_like(omega)

for i, w in enumerate(omega):
    G0 = G0_matrix(w)
    G0_inv = np.linalg.inv(G0)

    # Spin-up channel
    S_up = Sigma_up_matrix(w)
    G_up = np.linalg.inv(G0_inv - S_up)
    A_up[i] = -1/np.pi * np.imag(G_up[0,0])

    # Spin-down channel
    S_down = Sigma_down_matrix(w)
    G_down = np.linalg.inv(G0_inv - S_down)
    A_down[i] = -1/np.pi * np.imag(G_down[0,0])
```

7 Limiting Cases in the G_0W_0 Approximation

7.1 Non-interacting limit ($U \to 0$)

In the true non-interacting case the exact self-energy vanishes,

$$\Sigma_{\text{exact}}(\omega) \equiv 0,$$

so $G(\omega) = G_0(\omega)$ has only the two molecular-orbital poles at $\epsilon_0 \pm t$, each of weight $1/2$. However, in G_0W_0 the RPA polarizability

$$P(\omega) \; \propto \; \frac{1}{\omega^2 - (2t)^2}$$

retains poles at $\omega = \pm 2t$ even for $U \to 0$. Through

$$\Sigma(\omega) = i \int G_0(\omega - \omega')\, W(\omega')\, \frac{d\omega'}{2\pi},$$

with $W = U + UPU + \cdots$, these poles feed into $\Sigma(\omega)$ at $\omega = (\epsilon_0 \pm t) \pm 2t = \epsilon_0 \pm 3t$. Solving the Dyson equation $G^{-1} = G_0^{-1} - \Sigma$ yields zero-weight "satellite" poles at $\epsilon_0 \pm 3t$, which formally remain in G_{GW} even though their spectral weight vanishes as $\sim U^2 \to 0$.

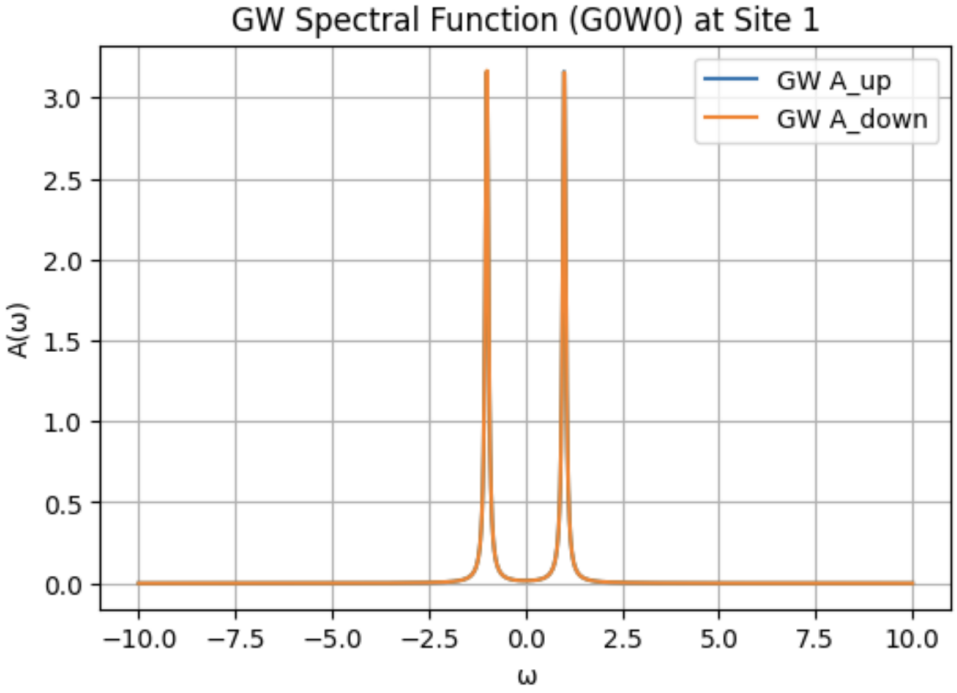

Figure 5: Two site Hubbard model at Quarter filling, GW approximation U=0.001, t=1, spin up and down spectral function.

7.2 Atomic limit ($t \to 0$, finite U)

Spin-up channel in the atomic limit ($t \to 0$) At quarter filling the dimer hosts a single $\uparrow$-electron and no $\downarrow$-electron. In the one-shot G_0W_0 approximation the spin-up self-energy splits into

1. A *Hartree* term $\Sigma_H^{\uparrow} = U\, n_{\downarrow}$, which vanishes since $n_{\downarrow} = 0$.
2. A *dynamic* term of order $U^2 t/h$, namely

$$\Sigma^{\uparrow}(\omega) = \frac{U^2\, t}{4h}\Big[\cdots\Big],$$

which scales linearly with t. Hence as $t \to 0$, $\Sigma^{\uparrow}(\omega) \to 0$.

Consequently, for the $\uparrow$ spin one has exactly

$$\Sigma^{\uparrow}(\omega) \;\to\; 0 \;\Longrightarrow\; G_{\uparrow}(\omega) = \big[G_0^{-1}(\omega) - \Sigma^{\uparrow}(\omega)\big]^{-1} \;\to\; G_0(\omega),$$

which in the atomic limit reduces to the single-pole form

$$G_0(\omega) = \frac{1}{\omega - \epsilon + i\eta}\,.$$

This coincides with the exact atomic-limit Green's function for the lone $\uparrow$ electron, so G_0W_0 reproduces the exact spin-up result as $t \to 0$.

Spin-down channel in the atomic limit ($t \to 0$) In the one-shot G_0W_0 approximation the spin-down self-energy decomposes into

- 1. A static Hartree shift
$$\Sigma_H^{\downarrow} = U\, n_{\uparrow} = U \cdot 1 = U,$$
but recall that in the standard G_0W_0 code we distribute this evenly over the two sites (or equivalently subtract half in G_0^{-1}), yielding an effective $\Sigma_H^{\downarrow} = \frac{U}{2}$.

  Why? In most GW implementations—whether for real materials or model Hamiltonians—the non-interacting Green's function G_0 is built from a mean-field Hamiltonian that already contains the static Hartree (or Hartree–Fock) potential. The GW self-energy $\Sigma_{\mathrm{GW}} = \Sigma_H + \Sigma_c$ is meant to correct *beyond* that reference, so one subtracts out (or "double-counts-corrects") any static piece already in G_0.

  - In our Hubbard-dimer code, G_0 was defined from
$$H_0 = -t \sum_{\langle ij \rangle} c_i^{\dagger} c_j \; + \; \epsilon \sum_i n_i$$
with *no* explicit Hartree term. Hence in the GW loop we must add back the full static Hartree shift $U\, n_{-\sigma}$.
  - However, one often centers frequencies so that the chemical potential (or half the total Hartree) sits at zero. Equivalently, you can *absorb* half of the static shift into a redefinition of G_0^{-1}, and let Σ_H contribute only the *excess* $\frac{U}{2}(n_{-\sigma} - 1)$. At quarter filling ($n_{\uparrow} = 1, n_{\downarrow} = 0$), this gives
$$\Sigma_H^{\downarrow} = U \cdot n_{\uparrow} \; - \; \frac{U}{2} \cdot (1 + 0) = \frac{U}{2}\,.$$
  - This "half-shift" convention is entirely analogous to how *ab initio* GW subtracts the DFT exchange–correlation potential: $\Sigma_{\mathrm{GW}} = \Sigma_H + (\Sigma_c - V_{xc}^{\mathrm{DFT}})$.

- 2. A dynamic (frequency-dependent) part
$$\Sigma_c^{\downarrow}(\omega) = \frac{U^2\, t}{4\, h}\Big[\cdots\Big], \quad h = \sqrt{(4t)^2 + U^2} \; \xrightarrow[t \to 0]{} \; U,$$
which vanishes linearly with $t \to 0$.

Hence in the limit $t \to 0$ one finds
$$\Sigma^{\downarrow}(\omega) \; \to \; \frac{U}{2},$$
so the GW Green's function reduces to a single–pole form
$$G_{\downarrow}(\omega) = \frac{1}{\omega - (\epsilon + \frac{U}{2}) + i\eta}\,.$$

By contrast, the exact atomic-limit solution for adding a ↓-electron to the one-electron ground state yields two poles at $\omega = \epsilon$ and $\omega = \epsilon + U$. Thus G_0W_0 (see fig 7 misses the correct two-peak "Hubbard-band" structure, collapsing the spin-down channel to a single, half-shifted pole at $\epsilon + U/2$.

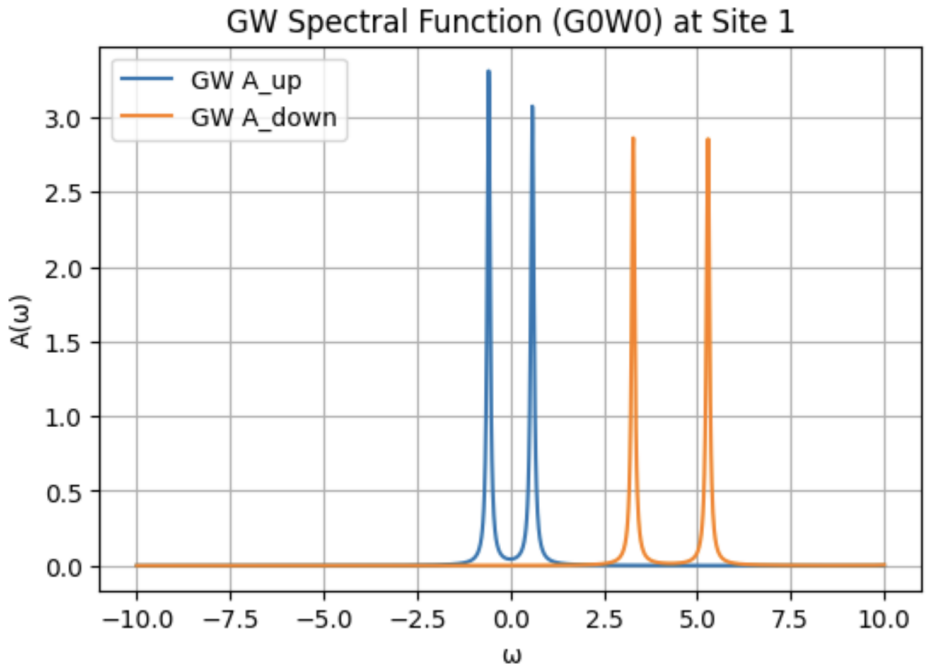

Figure 6: Two site Hubbard model at Quarter filling, GW approximation, U=10, t=1 spin up and down spectral function.

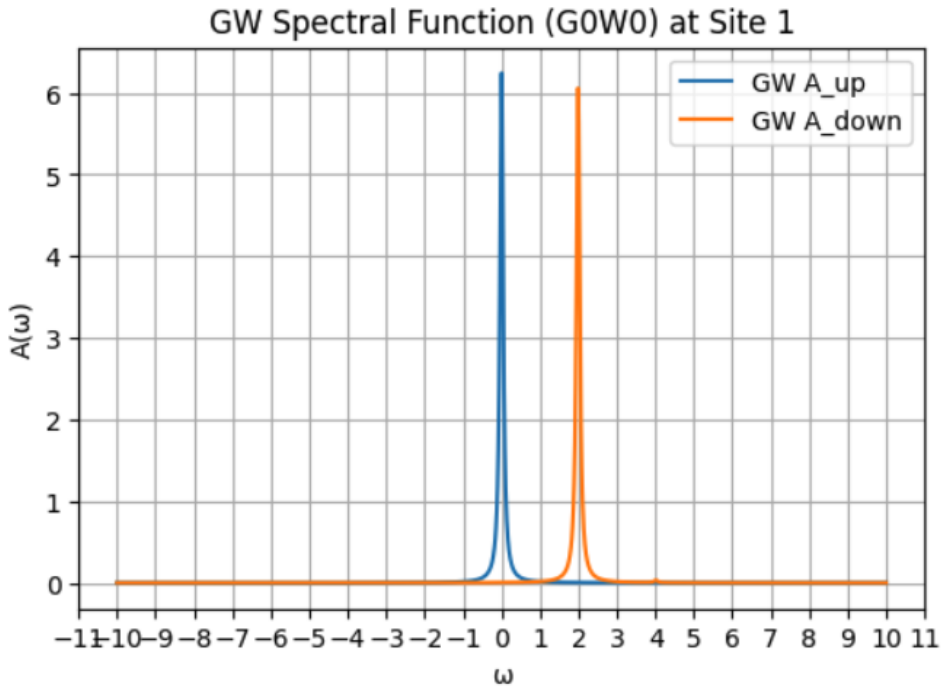

Figure 7: Two site Hubbard model at Quarter filling, GW approximation, U=4, t=0.1 spin up and down spectral function.

Origin of static vs. dynamic self-energy contributions The key distinction is that the "static" Hartree terms arise from the *instantaneous*, local mean-field generated by a pure on-site repulsion U, whereas the "dynamic" pieces involve virtual hops (amplitude t) and therefore carry nontrivial frequency dependence:

- **Hartree (static) term:** $\Sigma_H^\sigma = U\, n_{-\sigma}$ comes from the first-order diagram in which an electron of spin σ "sees" a frozen background charge $n_{-\sigma}$. No energy is exchanged in this process, so Σ_H^σ is independent of ω (static).
- **Dynamic (frequency-dependent) terms:** These first appear at second order in U and require a virtual excitation—an electron must hop (amplitude t), pay the interaction cost U, then hop back. In diagrammatic language this is the bubble (or exchange) diagram which carries internal propagators $\propto 1/(\omega - \text{energy})$. Because each virtual hop involves a factor of t and introduces an energy denominator $\omega - \ldots$, these contributions depend nontrivially on frequency and vanish as $t \to 0$.
- **Scaling:** - Hartree: $\Sigma_H \propto U\, n$, no ω. - Correlation: $\Sigma_c \propto U^2\, t/h$ with poles at $\omega \approx \epsilon \pm (t+h)$, so $\lim_{t\to 0} \Sigma_c(\omega) \to 0$ but Σ_H remains finite.

Thus the pure-U piece is an instantaneous mean-field shift (static), while any nonzero t is required to generate frequency-dependent (dynamic) self-energy structure.

8 Self-Consistent GW (scGW) for the Hubbard Dimer

One can extend the one-shot G_0W_0 scheme to a fully self-consistent GW by iterating both the Green's function and the RPA screening until convergence. In practice for the two-site dimer the

steps are:

1. **Initialize** Set the zeroth-order Green's function to the non-interacting one:

$$G^{(0)}(\omega) \;=\; G_0(\omega)\,.$$

2. **Compute polarization** Using the current $G^{(n)}$, form the RPA polarizability in the site basis

$$P_{ij}^{(n)}(\omega) = -\,i\sum_{\sigma}\int \frac{d\omega'}{2\pi}\, G_{ij}^{(n)\,\sigma}(\omega+\omega')\, G_{ji}^{(n)\,\sigma}(\omega').$$

3. **Update screened interaction** Build the dynamical W via

$$W^{(n)}(\omega) = U + U\,P^{(n)}(\omega)\,U \;+\; \cdots = \big[\,1 - U\,P^{(n)}(\omega)\big]^{-1}U.$$

4. **Compute self-energy** Convolve $G^{(n)}$ with $W^{(n)}$:

$$\Sigma_{ij}^{(n)\,\sigma}(\omega) = i\int \frac{d\omega'}{2\pi}\, G_{ij}^{(n)\,\sigma}(\omega-\omega')\, W_{ij}^{(n)}(\omega').$$

5. **Solve Dyson's equation** Obtain the next Green's function:

$$G^{(n+1)}(\omega) = \big[\,G_0^{-1}(\omega) \;-\; \Sigma^{(n)}(\omega)\big]^{-1}.$$

6. **Check convergence** Stop when $\|G^{(n+1)} - G^{(n)}\|$ or $\|\Sigma^{(n+1)} - \Sigma^{(n)}\|$ falls below a chosen tolerance.

Implementation notes.

- In the two-site model each of these objects (G, P, W, Σ) is a 2×2 matrix in site–space and can be sampled on the same frequency grid.
- The RPA-polarizability integral can be carried out analytically for each ω (generalizing the G_0 formulas) or evaluated numerically by quadrature.
- Convergence is typically reached in a few (5–10) iterations for moderate U/t.

Limitations. Although scGW enforces consistency and conserves particle number and energy, it still omits the vertex function Γ. Consequently phenomena requiring two-particle exchange channels—such as the superexchange splitting $J \sim 4t^2/U$ of the low-energy manifold—remain absent even in the self-consistent solution.

Unphysical Relaxation in Self-Consistent GW In the two-site Hubbard dimer at quarter filling, one-shot G_0W_0 with a static Hartree shift can sustain a spin-dependent spectrum, albeit approximate. However, when one enforces full self-consistency (scGW) without any vertex corrections, the iterative Dyson loop treats both spin channels through the same RPA-screened interaction. As a consequence, any seeded spin imbalance decays and the solution relaxes to a completely paramagnetic state with $G_\uparrow = G_\downarrow$. This unphysical collapse erases essential magnetic features—most notably the spin-dependent Hartree shifts and the superexchange splitting $J \sim 4t^2/U$—and leads

to spectral functions that are even more at odds with the exact dimer physics than the simpler G_0W_0 approximation.

Also note that the code provided does not really converge, this is due t the non-variational nature of GW. Unlike Hartree–Fock or DFT, GW is not derived from a minimum principle. The self-consistency map

$$G^{(n)} \;\mapsto\; G^{(n+1)} = (G_0^{-1} - \Sigma[G^{(n)}])^{-1}$$

need not be a contraction: multiple fixed points (paramagnetic, magnetic) can exist, and the iteration can oscillate or lock into a limit cycle.

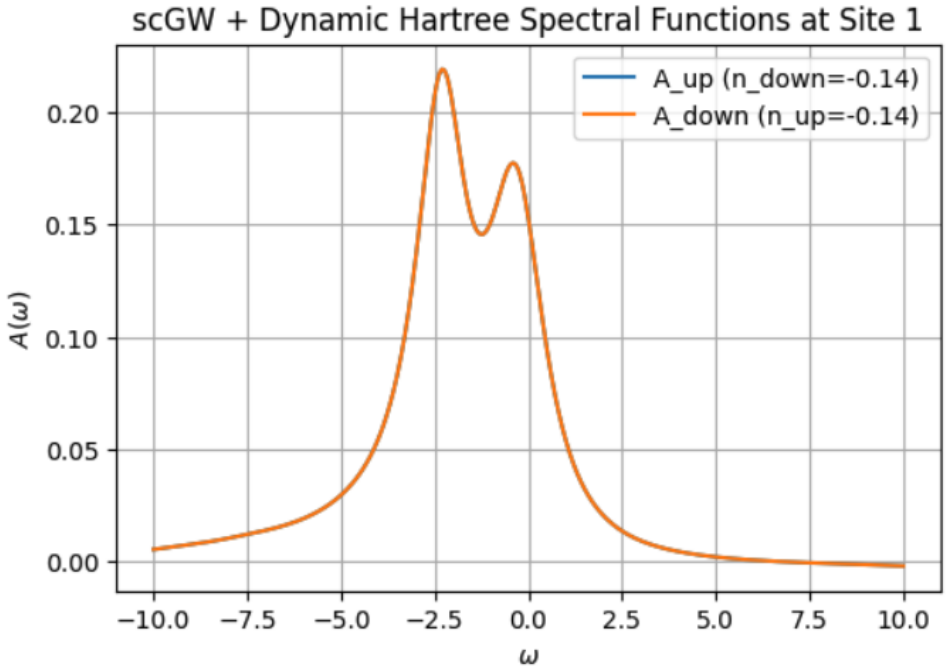

Figure 8: Two site Hubbard model at Quarter filling, U=4, t=1 spin up/down spectral function in scGW.